Diffusivity of hydrogen and properties of point defects in beryllium investigated by DFT

L. Ferry, F. Virot, Y. Ferro, D. Matveev, C. Linsmeier, M. Barrachin

Version of Record: https://www.sciencedirect.com/science/article/pii/S0022311519301278
Manuscript_3f8e72b772c5a97d3389c83df416726d

Diffusivity of hydrogen and properties of point defects in beryllium investigated by DFT

L. Ferry[a,b], F. Virot[a], Y. Ferro[b], D. Matveev[c], Ch. Linsmeier[c], M. Barrachin[a]

[a] *Institut de Radioprotection et de Sûreté Nucléaire (IRSN, PSN-RES/SAG), 13115 Saint Paul les Durance, France*
[b] *Aix-Marseille Univ., CNRS, PIIM, Marseille, France*
[c] *Forschungszentrum Jülich GmbH, Institut für Energie- und Klimaforschung - Plasmaphysik, Partner of the Trilateral Euregio Cluster (TEC), 52425 Jülich, Germany*

Abstract

Beryllium will be one of the plasma-facing materials for ITER. It will have to sustain high fluxes of hydrogen isotopes and as a consequence significant amounts of tritium can be retained in the wall. For safety and operational reasons, the deuterium and tritium inventory in the vacuum vessel must be limited. As a consequence, hydrogen diffusion, trapping and solubility are of vital importance in assessing and modeling the plasma fuel retention into the wall. In order to understand these issues, point defects and the behavior of hydrogen in beryllium are investigated based on Density Functional Theory calculations. Although some data have already been acquired in the past, some of them disagree, which motivates further investigations. To do so, the formation energy and diffusion properties of point defects are investigated in the first part of this paper. In a second part, the solubility and diffusivity of hydrogen in beryllium are calculated. A diffusion coefficient is established in order to be used in Rate-Equation and Kinetic Monte-Carlo Kinetic models and to allow for comparison with experimental measurements.

Keywords: ITER, hydrogen isotopes, beryllium, vacancy

1. Introduction

The ITER project [1–3] aims to demonstrate the technical and scientific feasibility of producing energy from nuclear fusion of deuterium and tritium. Beryllium has been chosen as the main plasma-facing material of the inner wall of ITER. However, beryllium could significantly retain hydrogen isotopes in the wall, this amount being dependent on the accumulated exposure fluence and on the surface temperature [4, 5]. The administrative limit on the amount of tritium in the vacuum chamber of ITER is currently fixed to 700g. As a consequence, it is essential to remove hydrogen's isotopes from the wall, which could be achieved by baking the beryllium tiles [6–9] of the inner-wall. The temperature dependency of the hydrogen release is not only important to limit the tritium inventory in normal conditions, but also to predict the behavior of tritium in case of confinement loss. As mentioned by Oberkofler [10], although much experimental data have been acquired on hydrogen retention and its transport in beryllium, the detail of the elementary processes is still not completely clear. Activation and binding energies are not directly accessible from experiment, but some of them have been provided by Density Functional Theory (DFT) calculations [11–14]. According to earlier results from Macroscopic Rate Equation (MRE) modeling acquired with the Coupled Reaction Diffusion System (CRDS) code [15, 16], a good agreement was found between experiment and modeling at the price of empirical adjustment of some parameters due to an insufficient knowledge of the processes. This highlights the fact that atomic scale mechanisms are still not well understood today. In particular, point-defects could significantly affect the retention properties of hydrogen in beryllium; among them are single (V_1) and di-vacancies (V_2) and single interstitial atoms (SIA). The diffusion properties of point-defects are also of importance in order to determine their evolution in time and their significance. Part of those properties were previously investigated but some inconsistencies were found, particularly regarding the diffusion properties. Even if we consequently paid a special attention to the numerical parameters used to attain convergency in the present work, these discrepancies are mostly the results of investigating different

Email address: francois.virot@irsn.fr (F. Virot)

migration paths. Among the discrepancies we noted are the diffusion of V_1, which was found isotropic in [14] with an activation energy of 0.72 eV, while it is anisotropic in [17] with activation energies of 0.72 and 0.89 eV. The same discrepancy exists for the diffusion of a SIA which is found isotropic [17] or not [14] depending on the authors.

As a consequence, the first aim of this paper is to carefully assess the energy of formation and the diffusion properties of a single-vacancy and a self-interstitial atom in beryllium, along with the relative stability of a single versus di-vacancies. The second aim is to establish a diffusion coefficient of hydrogen in perfect beryllium; this was achieved based on the DFT calculations presented in this paper. The diffusion coefficient we obtained is further compared with previous ones from experimental measurements made on beryllium sample with purities ranging from 98.0 % to 99.8 %.

In the end, this paper is organized as follows: the computational details of the DFT calculations are given in Section 2. Section 3 deals with point defects including SIA, V_1 and V_2. The hydrogen behavior in beryllium is investigated in Section 4 before a discussion and a conclusion are given in Section 5.

2. Methods

All the DFT calculations are performed with the Quantum Espresso code [18] using the Perdew, Burke, and Ernzerhof (PBE) exchange and correlation functional [19]. A full relaxation of the atomic positions was used in every case and the atoms were allowed to relax until the residual force fell below 0.003 eV/Å and the total energy below 0.001 eV. The volume of the supercell was kept constant during the optimization procedure. The vibrational properties are calculated with the Density Functional Perturbation Theory as implanted in Quantum Espresso [20]. The ZPE (zero-point energy) correction has however not been considered. It was shown to have a weak impact on the respective stability of different sites for H trapping and to induce weak corrections on the energy values in the range of 0.03 to 0.1 eV [21]. Nevertheless, ZPE is implicitly includes in the vibrational Helmoltz's free energy. We used a system size of $4 \times 4 \times 4$ unit cells containing 128 atoms, and a $5 \times 5 \times 5$ sampling of the Brillouin Zone (BZ). To check the stability of hydrogen (beryllium) atoms at interstitial sites, phonons calculations have been performed in a $3 \times 3 \times 3$ ($4 \times 4 \times 2$) supercell containing 54 (64) atoms, and a $6 \times 6 \times 6$ ($5 \times 5 \times 9$) sampling of the BZ. A cut-off in energy of 30 Ry on the wave-functions and the smearing scheme of Marzari-Vanderbilt [22] with a broadening value of 0.05 Ry were used. Activation energies were determined using the Nudged Elastic Band (NEB) method [23] incorporating the Climbing Image scheme (CI-NEB) [24]. The NEB calculations were considered converged once the norm of the forces orthogonal to the path are less than 0.05 eVÅ^{-1}. The parameters of the unit cell (Table 1) and other methodology details can be found in [25].

Table 1: Calculated and experimental beryllium properties.

Source	a (Å)	c (Å)	c/a	E_{coh} (eV/atom)	B (GPa)
Present	2.258	3.549	1.572	3.70	121
Exp.	2.286[1]	3.584[1]	1.568	3.32[2]	121[3]

[1] [26]
[2] [27–29]
[3] extrapolated at 0 K [30]

3. Point defects in beryllium

3.1. Monovacancies

The formation energy of a monovacancy ($\Delta_f E_{V_1}$) is a property that is very sensitive to the DFT convergence criteria used for the calculation [25]; $\Delta_f E^{V_1}$ is defined as:

$$\Delta_f E_{V_1} = E(N-1, 1V, N\Omega_0) - \frac{N-1}{N} E(N, 0V, N\Omega_0) \quad (1)$$

where $E(N-1, 1V, N\Omega_0)$ is the total energy of the defective supercell with volume $N\Omega_0$ containing $N-1$ atoms and one vacancy, and $E(N, 0V, N\Omega_0)$ is the total energy of the non-defective supercell containing N beryllium atoms. We found $\Delta_f E_{V_1} = 0.87$ eV with the DFT parameters previously given. Relaxing the volume only leads to a contraction of 0.1% of the 4×4×4 unit-cell while the energy remains the same within 0.01 eV.

The diffusion of a monovacancy is calculated along paths lying in and out of the basal plane Be(0001), with corresponding activation energies $E^{\ddagger}_{V_1,in}$=0.66 eV and $E^{\ddagger}_{V_1,out}$=0.83 eV. Consequently, the diffusion of V_1 is anisotropic in beryllium even if both *in* and *out* activation energies are of similar magnitude. This result is in good agreement with the findings of Middleburgh *et al.* [17] ($E^{\ddagger}_{V_1,in}$=0.72 eV and $E^{\ddagger}_{V_1,out}$=0.89 eV); on the contrary in Ref. [14], an isotropic process is found ($E^{\ddagger}_{V_1,in,out}$=0.72 eV). Two different experimental values are reported in the literature for *hcp* beryllium. Nicoud *et al.* [31, 32] estimated $E^{\ddagger}_{d} = 0.8$ eV from resistivity recovery measurements on neutron irradiated beryllium samples with incident energy of about 1 MeV and at low temperature (220-300 K). From a general point

of view, the resistivity recovery cannot discriminate between different types of defects. The Nicoud's value is derived from the assumption that only one type of defect (i.e. monovacacancy) governs the resistivity recovery in the experiment. Chabre *et al.* reported $E_d^{\ddagger} = 0.65$ eV [33] based on NMR (nuclear magnetic resonance) analysis between 300 and 1200K. The comparison between theory and experiment is satisfactory even if no indication from experiments are available regarding to the isotropic character of the diffusion process of a vacancy.

3.2. Divacancies

Six configurations are considered for the divacancy; they are displayed in Figure 1. The formation and dissociation energies are calculated as follows:

$$\Delta_f E_{V_2} = E(N-2, 2V, N\Omega_0) - \frac{N-2}{N} E(N, 0V, N\Omega_0) \quad (2)$$

$$\Delta_{\text{dis}} E_{V_2} = 2\Delta_f E_{V_1} - \Delta_f E_{V_2}, \quad (3)$$

Equation (3) implies that two monovacancies are more stable than one divacancy when $\Delta_{\text{dis}} E_{V_2}$ is negative. In Table 2, all dissociation energies are negative, indicating that at low temperatures and under thermodynamic equilibrium, the divacancy dissociates into two monovacancies. Taking the volume relaxation into account does not change this result since it leads to lower the formation energy by 0.1 eV with a volume contraction of 0.4% for the configuration shown in Figure 1(a). In case of a divacancy would be created by neutron bombardment, it can be assumed that it dissociates into two single vacancies; this is the reason why we did not evaluate the activation barriers for the diffusion of a divacancy. This result seems to be qualitatively in accordance with some observations performed on irradiated samples by neutrons (>1 MeV at 77 K) or by electrons (>2-3 MeV at 20 K), which stated that presence of vacancy aggregate is unlikely noting however that their electron microscopy resolution was limited to about 15 Å [31].

3.3. Self-Interstitial Atoms (SIAs)

Eight different self-interstitial configurations have been considerered in the present work. We labelled them the same way as Johnson and Beeler [34] (Figure 2): octahedral (O), tetrahedral (T), basal tetrahedral (BT), and basal octahedral (BO) interstitial sites, crowdions in (BC) and out (C) of the basal plane, and split dumbbells in (BS) and out (S) of the basal plane along the c axis. The interstitial formation energies are calculated as follows:

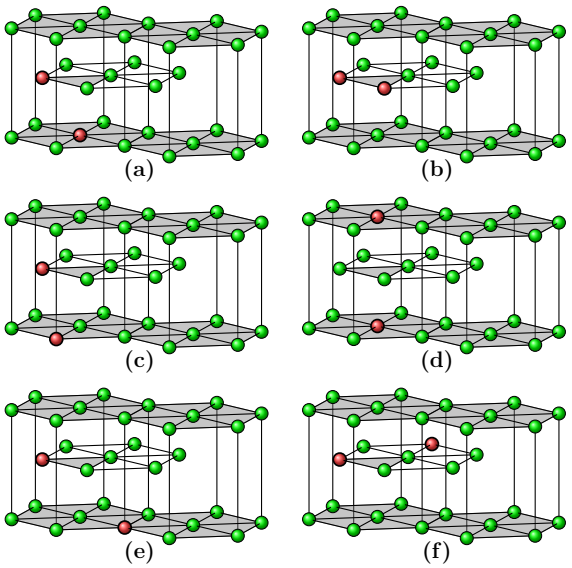

Figure 1: Configurations of divacancies considered in this work

Table 2: Formation and dissociation energies of divacancies, and distance between monovacancies

Config.	$\Delta_f E_{V_2}$ (eV)[1]	$\Delta_{\text{dis}} E_{V_2}$ (eV)	d(V–V) (Å)
(a)	2.05	-0.32	2.20
(b)	1.98	-0.24	2.26
(c)	2.08	-0.35	3.15
(d)	1.95	-0.22	3.55
(e)	1.88	-0.15	3.88
(f)	1.88	-0.15	3.91

[1] Comparison with the formation energy of two isolated monovacancies : 1.74 eV

$$\Delta_f E_{\text{SIA}} = E(N+1, 0V, N\Omega_0) - \frac{N+1}{N} E(N, 0V, N\Omega_0) \quad (4)$$

where $E(N+1, 0V, N\Omega_0)$ is the total energy of the defective supercell with $N+1$ atoms at volume $N\Omega_0$, and $E(N, 0V, \Omega_0)$ is the total energy of the non-defective supercell. The results are reported in Table 3.

Only three configurations are stable; they are O, C and BO. The formation energies of SIAs are much higher ($\simeq$ 4-5 eV) than the one of a monovacancy (0.87 eV). Consequently, SIA are not the dominant defect in beryllium. This result is not affected by taking the volume relaxation into account: it leads to a volume

Table 3: Formation energies (eV) of self-interstitials in configurations shown in Figure 2

Source	Configurations							
	O	T	S	C	BO	BT	BS	BC
Present work	5.27[1]	unst.[2]	unst.	4.46	4.20	unst.	unst.	unst.
Ganchenkova *et al.*[35]	5.24	5.22	5.29	4.39	4.20	unst.	4.30	unst.
Middleburgh *et al.*[17]	5.06[3]	5.14	nd.[4]	nd.	4.01	5.67[3]	nd.	nd.

[1] Metastable state according to phonons calculations
[2] Unst.: means that Be interstitial atom does not keep its initial position during the simulation
[3] Saddle point
[4] nd.: not determined

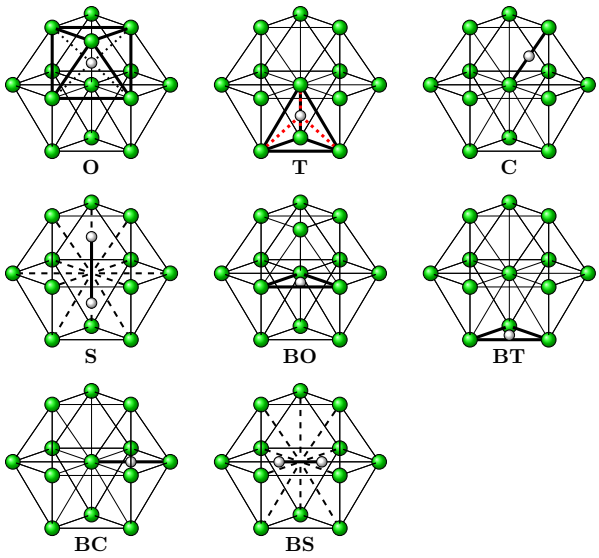

Figure 2: Eight interstitial configurations in *hcp* beryllium

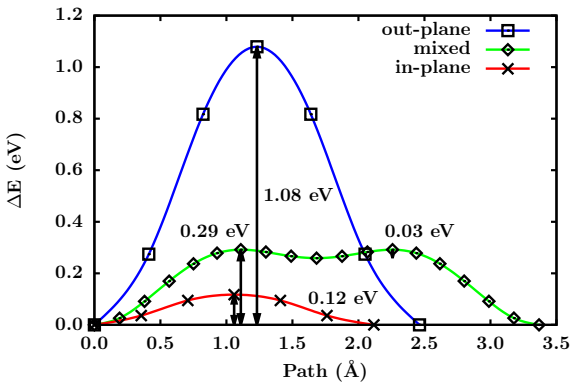

Figure 3: Migration energy profiles of a self-interstitial beryllium atom.The activation energy of 0.03 eV is related to migration from intermediate state to final one

swelling below 4% and lowers the formation energy by 4% for the BO configuration. They can nevertheless be produced by ion and/or neutron irradiation and, as a consequence, could play a role in the mechanisms leading to H trapping. This is why we paid attention to the migration of SIAs and considered different paths between BO sites, which are the most stable ones. Three diffusion mechanisms have been determined in the basal plane, out of the basal plane and a combination of both labelled *mixed*; the associated energy barriers are represented in Figure 3. For the diffusion path in the basal plane, we found an indirect interstitial mechanism in which a lattice Be atom is shifted by a SIA towards a BO site. The SIA should preferentially move along this direction since the activation energy for this process is very low: $E^{\ddagger}_{\mathrm{SIA,in}}$=0.12 eV. The diffusion out of the basal plane is a migration between two nearest neighbor BO sites in two consecutive basal planes. The energy barrier is much higher (1.08 eV) and the saddle point corresponds to an O site. A third migration pathway, so-called *mixed*, involves a diffusion in and out the basal plane. This process could be divided into two steps illustrated in Figure 4:

- The interstitial Be atom pushes a lattice atom into a C site.
- The Be atom in the C site moves upwards to the basal plane above where it pushes a lattice atom into the final BO site.

This last process has an energy barrier of $E^{\ddagger}_{\mathrm{SIA,mix}}$=0.29 eV with a local minimum at the C site.

The three different activation energies are not so easy to compare with the literature. Allouche [14] found similar energies (Table 4) but the mechanisms are not given.

Table 4: Comparison of diffusion energies at 0 K in beryllium with other works

Diffusing species	Direction of diffusion	$E_d^{\ddagger}$ (eV)		
		Present work	Allouche *et al.*[14]	Middleburgh *et al.*[17]
V_1	in-plane	0.66	0.72	0.72
	out-plane	0.83	0.72	0.89
SIA	in-plane	0.12	0.12	1.72 [1]
	out-plane	1.08	0.97	0.99
	mixed	0.29	0.30	0.64[1]

[1] See text for discussion

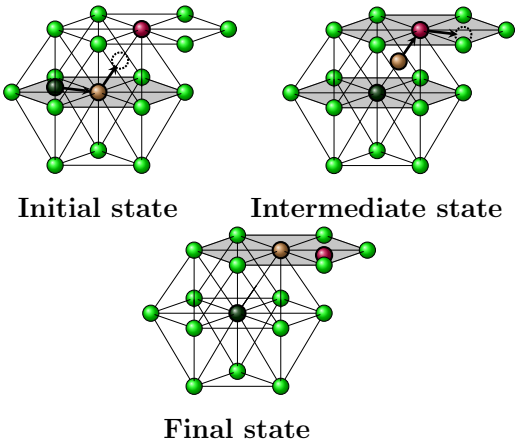

Figure 4: Schematic representation of the SIA migration according to the indirect mechanism

Middleburgh *et al.* [17] computed higher activation barriers according to different paths: through the BT site in-plane, and through the so-called NBt close to the C site for the *mixed* mechanism. Nevertheless, the activation barriers we calculated are among the lowest found up to now, which ensure we probably followed the minimum energy path. We can conclude that the diffusion of SIAs is dominated by an indirect mechanism that leads to very low activation barriers. Some experimental results also exist to compare with. Assuming an Arrhenius law, Dupouy [36] determined activation energies of 1.71 eV and 1.63 eV for the *in* and *out* mechanisms by means of the ^{7}Be radiotracer technique. Based on NMR [33], lower activation barriers were found, 1.35 and 1.40 eV, respectively. This is nevertheless higher than the energies we calculated. However, since SIA interact with vacancy, significant amount of SIA-vacancy recombinations are expected, leading to slowing down the global diffusion mechanism, and making the direct comparison with experiment not straightforward.

4. Hydrogen in non-defective beryllium

4.1. Hydrogen solubility

The positions, that hydrogen can adopt when located at interstitial sites, are the same as the SIA configurations shown in Figure 2, except the S and BS positions that can only be defined for a SIA. Geometry optimizations revealed that the T and BC sites are unstable in both cases, since the H atom moves spontaneously to the BT position. Phonon calculations displayed imaginary frequencies for the BO and C sites, meaning they are not located in a minimum in energy. In the end, only the BT and O sites are found to be stable trapping sites for hydrogen. The affinity between beryllium and hydrogen can be evaluated by the solution energy defined as follows:

$$\Delta_{\mathrm{sol}}E_H = E(N,H) - E(N) - \frac{1}{2}E(H_2) \qquad (5)$$

Table 5: Non-defective beryllium-solution energies (eV) of hydrogen in BT and O positions at 0 K in comparison with earlier studies (ZPE effects not included)

Source	BT	O
Present work [1]	1.67	1.87
Middleburgh [17][2]	1.40	1.59
Ganchenkova [35][3]	1.58	1.79
Zhang [21] [3]	1.55	1.76

[1] $\Delta_{dis}E_{H_2}$=4.52 eV
[2] $\Delta_{dis}E_{H_2}$=4.6 eV
[3] Value of $\Delta_{dis}E_{H_2}$ questionable

The solution energy we computed in the BT and O sites compare well with previous studies as shown in Table 5. The difference in energy between both BT and O sites is around 0.2 eV; it is the same as in previous works. The strongly positive value of the solution energy is indicative of a very low affinity of beryllium for hydrogen; a low solubility C^s follows, according to the Sievert's law:

$$C_s = C_{\mathrm{H,s}} \exp\left[-\frac{\Delta_{\mathrm{sol}} E_H}{k_b T}\right] \tag{6}$$

$C_{\mathrm{H,s}} \propto \sqrt{P_{H_2}}$ where P_{H_2} is the pressure of the dihydrogen gas phase in equilibrium with hydrogen in bulk beryllium [37]. The very low H solubility measured in beryllium [38–40] (few appm H/Be atm$^{\frac{1}{2}}$) is in qualitative agreement with this result.

4.2. Hydrogen diffusivity: activation barrier

The stable trapping site for hydrogen in hcp beryllium is the BT position. When diffusing into the material, hydrogen is expected to jump from a BT site to another BT site. As a hydrogen can also occupy the O site, the most probable diffusion path could a priori involve jumps between BT and O sites. The minimum energy path was calculated with the NEB approach; the path we found is described thereafter. In a first step, a hydrogen atom diffuses from the BT to O site via a transition state (TS). The activation energy from BT the top of the activation barrier at the transition state was calculated at $\mathrm{E}^{\ddagger}_{BT\rightarrow O}$=0.39 eV; the corresponding path length is $l_{BT\rightarrow O} = \sqrt{c^2/16 + a^2/3} = 1.577$Å. In a second step, the hydrogen atom follows the reverse path, from the O site to a BT site via a symmetrically equivalent TS as in the first step. The activation barrier was calculated at $\mathrm{E}^{\ddagger}_{O\rightarrow BT}$=0.19 eV and the path length is obviously the same as in the first step. This result is in good agreement with previous studies in which the diffusion was found isotropic and the activation barrier was calculated at 0.38 eV in Ref. [12], and 0.40 eV in Ref. [17, 21]. Only one author [14] found the diffusion anisotropic with activation barriers equal to 0.41 and 0.74 eV in // and $\perp$ directions, which is probably the consequence of using a too small unit cell. From the experimental side, activation energies for diffusion were determined at 0.15 eV by Tazhibaeva *et al.* [41], 0.19 eV by Jones *et al.* [40], 0.61 eV or 0.51 eV by Kizu *et al.* [42, 43] , and 0.29 eV to 0.36 eV depending on the grade of the sample by Abramov [44], the latter being in good agreement with the one we determined. In the following, we go further in the comparison with experimental data and establish a diffusion coefficient based on the DFT data shown above.

4.3. Hydrogen diffusivity: diffusion coefficient

The diffusion coefficient $D(T)$ (m^{2}s^{-1}) of hydrogen in a material is usually given in the form of an Arrhenius law:

$$D(T) = D_0 \exp \frac{-E^{\ddagger}_d}{k_B T} \tag{7}$$

Following Wert and Zener [45], the diffusion coefficient can be expressed as [46, 47]:

$$D = \frac{n}{2d} L^2 \Gamma_{BT} \tag{8}$$

where n is the number of nearest neighbor interstitial positions, d is the dimension of the system ($d = 3$ here), L the jumps length and Γ_{BT} (s^{-1}) is the jump frequency from a BT site to another one. Equation (8) is not valid anymore in the case of a diffusion process through a local minimum like in beryllium through the BT→O→BT path. In such a case, the diffusion coefficient can be derived following Wimmer *et al.* [48] and Klyukin *et al.* [49].

We consequently assumed an equilibrium takes place between the BT and O site before another jump occurs from the O site. This assumption leads to consider a steady state in which the forward and backward fluxes (J_{fd} and J_{bd} given below) between the BT and O sites are equal.

$$J_{fd} = \frac{1}{A}\left(\frac{6}{2} N_{BT} \Gamma_{BT} - \frac{6}{2} N_O \Gamma_O\right) \tag{9}$$

$$J_{bd} = \frac{1}{A}\left(\frac{6}{2} N_O \Gamma_O - \frac{6}{2} N_{BT'} \Gamma_{BT}\right) \tag{10}$$

In equations (9) and (10), A is an arbitrary section of diffusion. Following Klyukin's development [49], and using the first Fick's law, one finally obtained an expression for the diffusion coefficient of hydrogen in beryllium:

$$D = \frac{3}{2} L^2 \Gamma_{BT} \left[1 + \exp \frac{-\Delta G_{BT\rightarrow O}}{k_B T}\right]^{-1} \tag{11}$$

where $L = 2l_{BT\rightarrow O}$, and $\Delta G^{BT\rightarrow O}$ the Gibbs free energy difference between the BT and O sites. $\Delta G_{BT\rightarrow O}$ is further approximate as the energy difference $\Delta E_{BT\rightarrow O}$ between the BT and O sites as in [49]. A first approximation to the jump frequency Γ_{BT} that appears in Equation (11) is given by the Wert and Zener theory [45]:

$$\Gamma_{BT} = \nu \exp \frac{-E^{\ddagger}_{BT\rightarrow O}}{k_B T} \quad (12)$$

In Equation (12), ν (s^{-1}) is the frequency of vibration of the solute species in an interstitial position, and $E^{\ddagger}_{BT\rightarrow O}$ is the activation barrier $E^{\ddagger}_{d}$ of Equation (7). The frequency ν is:

$$\nu = \sqrt{\frac{E^{\ddagger}_{d}}{2m\lambda}} \quad (13)$$

where, λ is the distance between two interstitial sites and m is the mass of the diffusing atom or molecule. Using $\lambda = 2l_{BT\rightarrow O}$ and the deuterium mass, we obtained $D_0 = 1.3\times10^{-6}$ m^2s^{-1} in Equation (7), which is three orders of magnitude higher than the experimental value determined by Abramov [44] (Table 6). In this crude model, the vibration of the hydrogen atom is supposed independent of the beryllium network, which could explain the discrepancy with the experimental results.

Another estimate of the jump frequency can be obtained according to the Transition State Theory [48, 50, 51]. It takes the form:

$$\Gamma_{BT} = \frac{k_B T}{h} \exp \frac{-\Delta G^{vib}_{BT\rightarrow TS}}{k_B T} \exp \frac{-E^{\ddagger}_{d}}{k_B T} \quad (14)$$

in which h is the Planck constant, and $G^{vib} = -k_B T lnZ^{vib}$ is the vibrational Gibbs free energy with Z^{vib} the vibrational partition function of the system, and $\Delta G^{vib}_{BT\rightarrow TS} = G^{vib}_{TS} - G^{vib}_{BT}$.

The vibrational properties were determined for hydrogen's isotopes located at the BT, TS and O sites using the small displacement method as implemented in Phonopy tool [52] within a 4×4×3 supercell.

The phonon density of states computed at the *Gamma* point (q(0,0,0) of the BZ) highlights a localised doubly degenerate state at high frequency (1100 cm^{-1}); these states are mainly due to the deuterium vibrations in the basal plane of the beryllium network. These frequencies are well separated from the rest of the beryllium network that spans over 200-700 cm^{-1}. This should guarantee that these vibrational states are localized around hydrogen isotopes. We consequently chose a large enough supercell to avoid any interaction with the neighboring images. We nevertheless checked the impact of considering additional q-points on the convergence of the vibrational Helmoltz's free energy, $F^{vib}(T)$. Despite the computational effort, we extended the q-point sampling in one of the direction of the BZ. $F^{vib}(T)$ was consequently calculated within a q-point mesh of $1\times1\times1$, $1\times1\times2$ and $1\times1\times3$. The deviation we found for $F^{vib}(T)$ was not larger than 0.5% at 1000 K,which allowed us to conclude that phonon spectra calculated at Γ lead to almost converged Helmholtz's energies in the temperature range of interest. The thermodynamic quantities, $\Delta F^{vib}_{BT\rightarrow TS}$ and $\Delta F^{vib}_{BT\rightarrow O}$ are plotted in Figure 5. Within the harmonic approximation the latter corresponds to the vibrational Gibbs free energy.

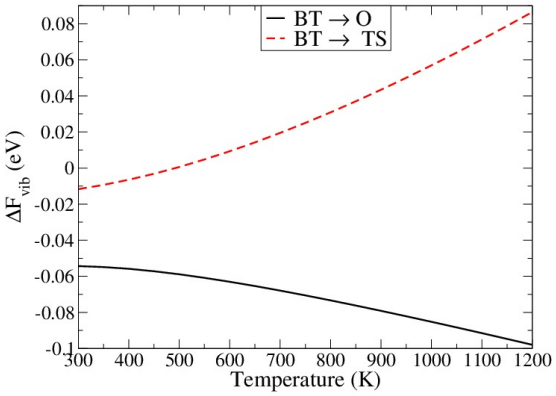

Figure 5: Vibrational Helmholtz energies required to calculate the diffusion coefficient of deuterium

The diffusion coefficient was then established based on Equations (11) and (14), and plotted in Figure 6 along with experimental results for comparison. The pre-exponential factor D_0 and the activation barrier E_d of Equation (7) were fitted with an Arrhenius law from 300 K up to 1200 K for both models. Parameters are reported in Table 6 for H, D and T. Despite that the model based on transition state theory is more sophisticated than one based on the Wert and Zener theory, both results get same results regarding to the diffusion coefficient in the temperature range of 300-1200 K.

It is to be noted that the experimental results are very scattered over several orders of magnitude, highlighting the large uncertainty with which the diffusion coefficient has been experimentally determined. The diffusion coefficient we determined clearly appears as un upper bound of the experimental results. This could be due to the fact that, at low temperature, the diffusion of hydrogen is experimentally slowed down by the presence of defects and other impurities. This behavior was already point out in tungsten [53–56] where two different diffusion regimes were observed depending on the temperature. Such a mechanism would explain the variation of the diffusion coefficient depending on the level of impurity or defects contained in the sample despite the fact that the large experimental uncertainty is probably also

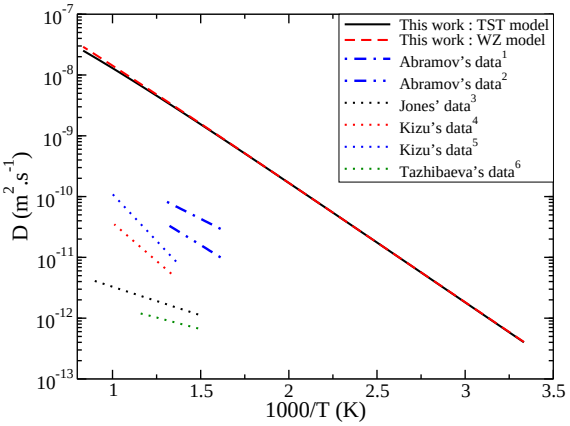

Figure 6: Diffusion coefficient determined by experiment and in this work following the Wert and Zener (WZ) model and the transition state theory (TST) plotted in red dashed and black lines, respectively. [1]Sample purity: 99.8% [44] ,[2] sample purity: 99% [44], [3] [40],[4] [43], [5][42], [6][41]

Table 6: Arrhenius parameters for the diffusion coefficient of hydrogen isotopes in non-defective beryllium

	Isotope	D_0 [m^2s^{-1}]	$E_d^{\ddagger}$ [eV]
Equations (11) and (12)	H	1.8×10^{-6}	0.38
	D	1.3×10^{-6}	0.38
	T	1.0×10^{-6}	0.38
Equations (11) and (14)	H	1.4×10^{-6}	0.38
	D	1.1×10^{-6}	0.38
	T	9.2×10^{-7}	0.38
Abramov *et al.*[44]	D	6.7×10^{-9}	0.29
Abramov *et al.*[44]	D	8.0×10^{-9}	0.36
Jones *et al.*[40]	T	2.9×10^{-11}	0.19
Kizu *et al.*[43]	H	1.3×10^{-8}	0.51
Kizu *et al.*[42]	H	1.3×10^{-7}	0.61
Tazhibaeva *et al.*[41]	D	9.0×10^{-12}	0.15

the consequence of the short range of temperature over which the measurements were performed.

5. Conclusions

In this paper, we investigated the formation energy, the diffusion properties of point defects along with the hydrogen behavior in perfect beryllium. We first clarified some of the mechanisms that involve point defects: the diffusion of a single vacancy is anisotropic in beryllium with activation barriers of 0.66 eV and 0.83 eV in direction in and out of the basal plane, and the diffusion of a SIA is isotropic with a very low activation barrier of 0.12 eV, meaning that a SIA diffuses nearly freely in perfect beryllium. We further established that di-vacancies are unstable with regard to single vacancies, at least at low temperature. In the end, we derived a diffusion coefficient for hydrogen; the activation barrier is in good agreement with some of the previous experimental studies, while the pre-factor is several orders of magnitude above the experimental results that are themselves scattered over several orders of magnitude. Some additional works, specifically focused on the effect of impurities, will be required in order to understand the difference between the diffusion coefficient herein calculated for hydrogen in perfect beryllium and the one measured experimentally on sample of diverse purities.

6. Acknowledgements

This work is supported by Région PACA. It has also been carried out within the framework of the EUROfusion Consortium and French Research Federation for Fusion Studies and has received funding from the Euratom research and training programme 20142018 under grant agreement No. 633053. The views and opinions expressed herein do not necessarily reflect those of the European Commission.

References

[1] J. Wesson, Tokamaks, third ed., Oxford University Press, 2004.
[2] A. Loarte, et al., Nucl. Fusion 47 (2007) S203.
[3] S. Brezinsek, et al., Nucl. Fusion 57 (2017) 116041.
[4] R. Causey, G. Longhurst, W. Harbin, J. Nucl. Mater. 241 (1997) 1041–1046.
[5] I. Kupriyanov, G. Nikolaev, V. Vlasov, A. Kovalev, V. Chakin, J. Nucl. Mater. 367-370, Part A (2007) 511–515.
[6] M. Baldwin, et al., J. Nucl. Mater. 337 (2005) 590.
[7] K. Sugiyama, et al., J. Nucl. Mater. 415 (2011) S731.
[8] R. Doerner, et al., J. Nucl. Mater. 257 (1998) 51–58.
[9] F. Scaffidi-Argentina, G. Piazza, R. Rolli, Fusion Eng. Des. 69 (2003) 505–509.
[10] M. Oberkofler, M. Reinelt, Linsmeier, Ch., Nucl. Instr. Meth. B 269 (2011) 1266–1270.
[11] M. Ganchenkova, V. Borodin, Phys. Rev. B 75 (2007) 054108.
[12] M. Ganchenkova, V. Borodin, R. Nieminen, Phys. Rev. B 79 (2009) 134101.
[13] P. Zhang, J. Zhao, B. Wen, J. Phys.: Condens. Matter 24 (2012) 095004.
[14] A. Allouche, M. Oberkofler, M. Reinelt, Linsmeier, Ch., J. Phys. Chem. C 114 (2010) 3588.
[15] R. Piechoczek, M. Reinelt, M. Oberkofler, A. Allouche, Linsmeier, Ch., J. Nucl. Mater. 438 (2013) 1072.
[16] D. Matveev, et al., Nuclear Inst. Method Phys. Res. B 430 (2018) 23.

[17] S. Middleburgh, R. Grimes, Acta Mater. 59 (2011) 7095.
[18] P. Giannozzi, et al., J. Phys.: Condens. Matter 21 (2009) 395502.
[19] J. Perdew, K. Burke, M. Ernzerhof, Phys. Rev. Lett. 77 (1996) 3865.
[20] S. Baroni, S. De Gironcoli, A. Dal Corso, P. Giannozzi, Rev. Mod. Phys. 73 (2001) 515.
[21] P. Zhang, J. Zhao, B. Wen, J. Nucl. Mater. 423 (2012) 164.
[22] N. Marzari, D. Vanderbilt, A. De Vita, M. Payne, Phys. Rev. Lett. 82 (1999) 3296.
[23] G. Henkelman, B. P. Uberuaga, H. Jónsson, J. Chem. Phys. 113 (2000) 9901–9904.
[24] M. Methfessel, A. Paxton, Phys. Rev. B 40 (1989) 3616.
[25] L. Ferry, et al., Nucl. Mater. Ener. 12 (2017) 453.
[26] K. Mackay, N. Hill, J. Nucl. Mater. 8 (1963) 263.
[27] R. Hultgren, et al., Selected Values of the Thermodynamic Properties of the Elements, Vol. 1, American Society for Metals, Metals Park, Ohio 44073, 1973.
[28] M. Chase, et al., J. Phys. Chem. Ref. Data 14.
[29] L. Gurvich, I. Veyts, C. Alcock, Thermodynamic Properties of Indiviudal Substances, fourth ed., Hemisphere Publishing Corporation, 1989.
[30] A. Migliori, H. Ledbetter, D. Thoma, T. Darling, J. Appl. Phys. 95 (2004) 2436.
[31] J. Nicoud, J. Delaplace, J. Hillairet, D. Schumacher, Y. Adda, J. Nucl. Mater. 27 (1968) 147.
[32] J. Nicoud, Contribution à l'étude des défauts créés dans le bryllium et le magnésium par irradiation à basse température, Ph.D. thesis, Université d'Orsay (1970).
[33] Y. Chabre, J. Phys. F: Met. Phys. 4 (1974) 626.
[34] R. Johnson, J. Beeler, Interatomic Potentials and Crystalline Defects, AIME, New York, 1981.
[35] M. Ganchenkova, P. Vladimirov, V. Borodin, J. Nucl. Mater. 386 (2009) 79.
[36] J. Dupouy, J. Mathi, Y. Adda, Mem. Sci. Rev. Met. 63 (1966) 481.
[37] Y. Fukai, The Metal-Hydrogen System: Basic Bulk Properties, Vol. 21, Springer Science & Business Media, 2006.
[38] V. Shapovalov, Y. Dukel'skii, Russian Metallurgy 5 (1988) 201–203.
[39] W. Swansiger, J. Vac. Sci. Technol. A4 (1986) 1216–1217.
[40] P. Jones, E. Gibson, Hydrogen in beryllium, J. Nucl. Mater. 21 (1967) 353.
[41] I. Tazhibaeva, et al., Proc. of the 18th symposium on Fusion technology (1994) 427.
[42] K. Kizu, K. Miyazaki, T. Tanabe, Fusion Technology 28 (1995) 1205.
[43] K. Kizu, T. Tanabe, in: Proceedings of 2nd International Workshop on Tritium Effects in Plasma Facing Components, 1994, p. 76.
[44] E. Abramov, M. Riehm, D. Thompson, W. Smeltzer, J. Nucl. Mater. 175 (1990) 90–95.
[45] B. Wert, C. Zener, Phys. Rev. 76 (1949) 1169.
[46] S. Elliot, The physics and chemistry of solids, Willey, 1998.
[47] C. Zener, J.Appl. Phys. 22 (1951) 372.
[48] E. Wimmer, W. Wolf, J. Sticht, P. Saxe, Phys. Rev. B 77 (2008) 134305.
[49] K. Klyukin, M. Shelyapina, D. Fruchart, J. Alloys Compd. 644 (2015) 371.
[50] G. Vineyard, J. Phys. Chem. solids 3 (1957) 121.
[51] K. Kehr, Theory of the diffusion of hydrogen in metals, Springer, 1978.
[52] A. Togo, I. Tanaka, Scr. Mater. 108 (2015) 1–5.
[53] K. Heinola, T. Ahlgren, J.Appl. Phys. 107 (2010) 113531.
[54] R. Frauenfelder, J. Vac. Sci. Technol. 6 (1969) 388.
[55] N. Fernandez, d. K. D. Ferro, Y. an, Acta Materialia 94 (2015) 307.
[56] T. Oda, D. Zhu, Y. Watanabe, J. Nucl. Mater. 467 (2015) 439.